Zaykovite, Rh_3Se_4, a new mineral from the Kazan placer (South Urals, Russia)

Elena V. Belogub[1*], Sergey N. Britvin[2,3], Vladimir V. Shilovskikh[2], Leonid A. Pautov[1,4], Vasiliy A. Kotlyarov[1], Elisaveta V. Zaykova[1]

[1] South Urals Federal Research Center of Mineralogy and Geoecology, Uralian Branch of Russian Academy of Sciences, Miass, 456317, Russia

[2] Saint-Petersburg State University, Universitetskaya Emb. 7/9, Saint Petersburg, 199034, Russia

[3] Nanomaterials Research Center, Kola Science Center of the Russian Academy of Sciences, Fersman Str. 14, 184209 Apatity, Russia

[4] Fersman Mineralogical Museum of the Russian Academy of Sciences, Leninsky Pr. 18-2, Moscow, 115162, Russia

Corresponding author: Elena V. Belogub (belogub_e@yahoo.com)

Abstract Zaykovite, ideally Rh_3Se_4, is a new mineral, the first natural rhodium selenide. It was discovered in the assemblages of platinum-group minerals from the Kazan gold placer, South Urals, Russia. The mineral occurs as crystals up to 40 μm in size within the grains of Pt3Fe alloy, in association with unnamed Pd-Sb-Te phase and Au-Pd alloy. In reflected light, zaykovite has a gray color with bluish-greeenish tint; it shows weak bireflectance and anisotropy. Reflectance values [R_{max}/R_{min} (%) for COM approved wavelengths (nm)]: 30.1/29.3(470), 32.2/31.0(546), 33.4/32.0(589), 35.1/33.7(650). Chemical composition corresponds to the empirical formula $(Rh_{2.26}Pt_{0.46}Ir_{0.25}Ru_{0.01}Pd_{0.01}Fe_{0.01})_{\Sigma 3.00}(Se_{2.77}S_{1.21}Te_{0.02})_{\Sigma 4.00}$ Zaykovite is monoclinic, space group *C*2/*m*, *a* 10.877(1), *b* 11.192(1), *c* 6.4796(6) Å, β 108.887(2)°, *V*

This is a 'preproof' accepted article for Mineralogical Magazine. This version may be subject to change during the production process.
DOI: 10.1180/mgm.2022.122

746.3(1) Å^3, Z = 6, D_{calc} 8.32 g cm^{-1}. The crystal structure has been solved and refined to R_1 = 0.016 based on 858 unique observed reflections. The strongest lines of the X-ray powder diffraction pattern [d(Å), (I), (hkl)] are: 5.43(37)(-111), 3.275(75)(310), 3.199(100)(-131), 3.061(87)(002), 2.568(62)(400), 2.545(41)(041), 3.413(34)(-241), 1.697(34)(441). Zaykovite is a Se analogue of kingstonite, Rh_3S_4. A continuous series of solid solutions between kingstonite and zaykovite was encountered in the assemblages of the Kazan placer. The possible sources of unique Rh-Se mineralization at South Urals could be serpentinised dunite-harzburgite or gabbro-clinopyroxenite-dunite complexes in the vicinity.

Key words. Platinum group mineral, rhodium, selenide, crystal structure, EBSD, gold placer, South Urals

Introduction

Rhodium and selenium are the rare elements with a different geochemical fate and, as a consequence, a low probability to be combined into rhodium selenide minerals. Platinum-group elements (PGE) are constituents of more than 20 selenides from the different localities worldwide (e.g., Johan et al., 1970; Davis et al., 1977; Jebwab et al. 1992; Cook et al. 1994; Polekhovskiy et al. 1997; Paar et al., 1998; Roberts et al., 2002; Vymazalová et al., 2012; Zaykov et al., 2017; Barkov et al., 2021; Krivovichev, 2021). However, the only natural rhodium selenide reported to date is a poorly defined phase with an inferred formula $(Rh,Cu)_9(Se,S)_{11}$, described from chromitites of the Luobusa ophiolite deposit, Tibet, China (Bai et al., 2007).

The high abundance of rhodium minerals in the PGM-bearing gold placers of South Urals, Russia, was established at the end of the last century, upon the discovery of polkanovite, $Rh_{12}As_7$, palladodymite, $(Pd,Rh)_2As$, and miassite, $Rh_{17}S_{15}$ (Britvin et al., 1998, 1999, 2001). The PGE mineralogy of ultramafic rocks and placers of the Uralian Platinum Belt located along the Main Uralian Fault mainly in the Middle Urals is well studied (e.g., Stepanov et al., 2019, 2020) (Fig. 1). The Rh-bearing species are represented by minerals of the kashinite–bowieite series and Ir–Rh–Pt thiospinels related to the cuproiridsite–cuprorhodsite–malanite series

https://doi.org/10.1180/mgm.2022.122 Published online by Cambridge University Press

(Tolstykh et al., 2011, 2015; Malich et al., 2015; Stepanov et al., 2019, 2020; Palamarchuk et al., 2020). Hollingworthite is known as secondary mineral developed after primary Pt–Fe alloys in the Nizhny Tagil and Kamenushensky massifs (Tolstykh et al., 2011, 2015). Cuprorhodsite occurs among platinum-group minerals of the Nizhny Tagil and the Veresovy Bor massifs (Begizov and Zav'yalov, 2016). Rhodplumsite $Rh_3Pb_2S_2$ and an unnamed telluride $(Pb,Bi)Rh_2Te_3$ were described from the Veresovyy Bor (Stepanov et al., 2020). However, neither selenide mineralization nor even selenium impurities in PGM of the primary and placer associations were reported in the deposits belonging to the Uralian Platinum Belt (Stepanov et al., 2020). The PGE mineralogy of the South Urals is much less studied (Saveliev et al., 2017; Zaykov et al., 2011, 2012, 2017; Zaykova et al., 2020; Rakhimov et al., 2021a, 2021b). Along with Rh minerals from the Miass river placers (Britvin et al., 1998, 1999, 2001), only kashinite with traces of Rh was described in chromitite from the Vladimir deposit of the Varshav ultramafic massif (Ankushev et al., 2016). Selenium-bearing PGMs were first discovered by Victor Zaykov (Zaykov et al., 2017) as microinclusions of sulfides and sulfoarsenides hosted by native platinum and Ir-Os alloys from the Kazan, Malo-Iremel and Bayramgulov gold placers (the Ingul placer area) (Zaykov et al., 2017; Belogub et al., 2020).

The Kazan placer was found to be most enriched in Se-PGE minerals. In the course of an ongoing research of the Kazan PGE assemblages, a new rhodium selenide, ideally Rh_3S_4, was discovered in this placer. The mineral is named zaykovite, in honor of Victor Vladimirovich Zaykov (1938–2017), Russian geologist and geoarchaeologist, for his contributions to the study of PGE minerals from gold placers of the Urals and other regions (Ankushev et al., 2016; Zaykov et al., 2017; Artem'ev et al., 2018). Both the mineral and its name have been approved by the Commission on New Minerals, Nomenclature and Classification of the International Mineralogical Association (IMA 2019-084).

Materials and Methods

https://doi.org/10.1180/mgm.2022.122 Published online by Cambridge University Press

Heavy mineral concentrates enriched with PGM were given to Victor Zaikov by A.Yu.Ivanov and B.Ya.Hismatullin (OOO (limited company) «Miasskiy priisk»). The sample was collected in open pit No.3 of the Kazan placer in July, 2017.

Chemical composition of zaykovite was determined using scanning electron microscope (SEM) with energy-dispersive analysator (EDA) Oxford link REMMA 2M, acceleration voltage = 20 kV; beam current = 6 nA; beam diameter = 2 μm, reference materials metallic Rh, Pt, Os, Ir, Ru, Pd, Au, Ag for respective metals, chalcopyrite (S, Fe, Cu), CdSe and Bi_2Se_3 (Se), set of standards NERMA.GEOL.25.10.74, Kyiv, 2005 at the South Urals Federal Research Center of Mineralogy and Geoecology and an electron microprobe JEOL JCXA-733 with wave dispersive spectrometer (WDS) using an acceleration voltage of 20 kV; a beam current of 20 nA; a beam diameter of 2 μm, reference materials metallic Rh, Pt, Ir, Ru, Pd for respective metals, pyrite (S, Fe), Bi_2Se_3 (Se) and HgTe (Te) at the Fersman Mineralogical Museum.

Formulae were calculated for 7 atoms (kingstonite-zaykovite series), 15 atoms (Pd-Sb-Te phase), and 1 atom (Pt-Fe and Au-Pd alloys).

Element distribution maps and additional data on chemical composition were obtained at the Geomodel Resource Center (Saint Petersburg State University (SPbU), St Petersburg, Russia) on a Hitachi S-3400N SEM equipped with an Oxford Instruments X-Max 20 EDA at an accelerating voltage of 10 kV and a beam current of 1 nA spatial resolution. The spectrometer was calibrated against a set of standard natural and synthetic samples, (Micro-Analysis Consultants Ltd (MAC) standards).

The electron backscattered diffraction (EBSD) maps were obtained using an Oxford Instruments HKL NordlysNano detector (Geomodel Resource Center, Scientific Park, SPbU) mounted on the abovementioned SEM. The acquisition conditions were as follows: 30 kV and 1.5 nA, an exposition of 0.5 s per pattern, averaging 5–10 images (when mapping) or 20 images (to obtain individual patterns), and their subsequent processing using the software package Oxford Instruments Channel5. Kingstonite crystal structure data (AMCSD № 0014575) was used for the comparison, isoferroplatinum (ICSD 56275), platinum (ICSD 76153) and mertieite-II (Karimova et al, 2018) structure data were used as references for EBSD mapping.

https://doi.org/10.1180/mgm.2022.122 Published online by Cambridge University Press

Data on the orientation of the individual crystals of zaykovite are shown in Euler color schemes, pole figures and orientation distribution density heatmaps (Mason and Schuh, 2009).

To obtain a mechanically undistorted surface, the sample for EBSD analysis was treated with a direct beam of Ar plasma using an Oxford Instruments Ionfab300 etcher, an exposition of 10 min, an angle of 45, an accelerating voltage 500 V, a current of 200 mA, and a beam diameter of 10 cm (Nanophotonics Resource Center, Scientific Park, SPbU).

Reflectance data for zaykovite were obtained using a microscope-spectrophotometer LOMO MSP-R equipped with a spectrophotometric attachment PEI ”R928” (Hamamatsu, Japan) at the South Urals Federal Research Center of Mineralogy and Geoecology, Miass, Russia. The measurements were done in air using a x40 objective with a 0.65 numerical aperture: a photometric diaphragm of 0.3 mm; a size of analyzing area of 0.007 mm; a diffraction grating of 600 grooves/mm; a spectral interval of 6 nm; a voltage of 450 V and elemental silicon as a standard. The measurements were provided for the 400-700 nm range.

Zaykovite grain used for the single-crystal study was extracted from the Pt-Fe alloy matrix manually, by gentle indentation of the adjacent metal with tungsten carbide needle. Single-crystal data were collected by means of a Bruker Kappa APEX DUO CCD diffractometer using Mo*K*α radiation. Data collection and integration procedures were performed using Bruker APEX2 and Bruker SAINT software (Bruker Inc., Wisconsin, USA). The crystal structure of zaykovite was solved by dual space method and refined to R_1 = 0.0158 using *SHELX*-2014 set of programs (Sheldrick, 2015) *via* Olex2 v.1.2.8 graphical user interface (Dolomanov et al., 2009). For mixed site occupancies, we used scattering factors of neutral atoms for Rh and Pt (sites *M*1-*M*4) and Se and S (sites *X*1-*X*4). Data collection and structure refinement details can be retrieved from the crystallographic information file (CIF) in Supplementary Materials.

X-ray powder diffraction data were obtained using a Rigaku R-AXIS Rapid II diffractometer with a curved (cylindrical) imaging plate detector (r = 127.4 mm). Co*K*α radiation (λ = 1.79021 Å); rotating anode (40 kV, 15 mA) with microfocus optics; a Gandolfi method with an exposure time of 60 min. The image-to-profile data conversion was completed using osc2xrd program (Britvin et al., 2017). Theoretical pattern was calculated on the basis of atomic coordinates obtained from the structure refinement and unit-cell parameters refined from the

https://doi.org/10.1180/mgm.2022.122 Published online by Cambridge University Press

powder diffraction data, by means of STOE WinXPOW software (Stoe & Cie GmbH, Darmstadt, Germany). Calculated lines having the intensity less than 2 have been omitted.

Geological background for the Kazan gold placer

Zaykovite was found in a heavy mineral concentrate obtained from the Kazan gold-bearing placer, which is a part of the Gogino placer zone, (Zaykov et al., 2017), 52° 42’ 00’’ N, 60° 26’ 27’’ E.

The Gogino placer zone is located in 100–150 km to the SSE from the city of Magnitogorsk in the Chelyabinsk region (Fig. 1) and includes ~20 placers, represented by the Mesozoic and Miocene karst and eluvial placers, 1.0–3.0 km long and 80–200 m wide. Most productive karst placers produced more than 2 t for the period 1851-2004 of gold with 925–901‰ fineness (unpublished reports of Ivanishchev et al., 2005). Native gold grains are mostly small and poorly rounded, which is indicating proximity to the source (Zaykov et al., 2017).

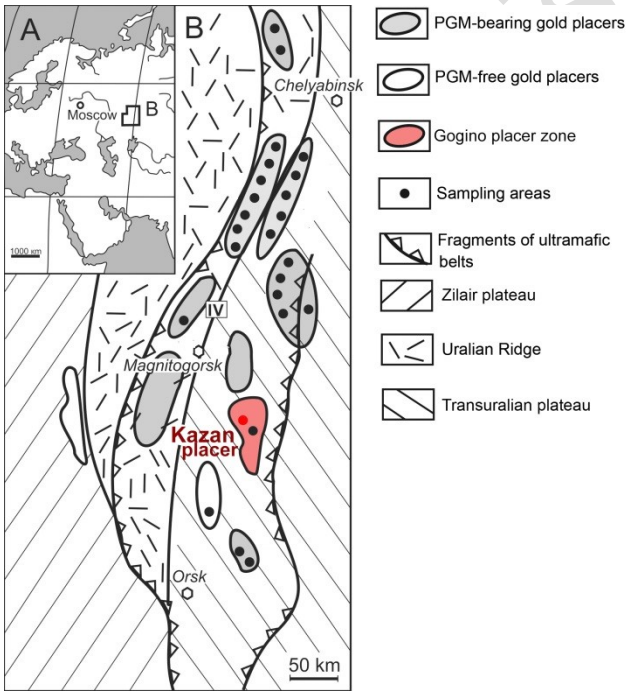

Fig. 1. Geographic setting of the South Urals (a) and location of the main placer zones and placers with data on the placer mineral assemblages (b) (simplified after Zaykov et al., 2017). Gogino placer zone and the Kazan placer are marked.

https://doi.org/10.1180/mgm.2022.122 Published online by Cambridge University Press

The Kazan placer is localized in the Bredy erosion-structural depression of the Cenomanian – Upper Pleistocenene age (Fig.2 a). It is located at the confluence of the Karagayly-Ayat and Kamyshly-Ayat rivers. The length of the placer exceeds 4 km with a highly variable width and a complex nesting-streamy morphology. There are no permanent watercourses in close proximity to the placer. The thickness of peat is from 1.5 to 35 m, sands from 0.2 to 4.3 m. The raft is represented by karsted Lower Carboniferous limestone (Figure 2 b). The Varshavka and Gogino ultramafic massifs are nearest potential sources for platinum-group minerals (PGM) in the placer.

The placer was exploited during 1851-1910. In 1996, exploitation was restarted (unpublished report of the Geological Survey of Chelyabinsk Geological Committee).

It was previously established that the heavy mineral concentrate of the Kazan placer mainly consists of chromite, platinum alloy (min-max-mean, wt.%): Pt 76-93-90.3, Fe 2.6-9.8-7.4, Cu 0.2-4.0 and gold alloy with a fineness of 780-1000, mean ~890-900 (Zaykova et al., 2020). Pt-Fe alloys grains constitute up to 73% of all PGMs in the heavy mineral concentrate. Native metals (gold alloys and alloys of the system Os-Ir-Ru, laurite-erlichmanite, sulfarsenides (irarsite, hollingworthite), stibiopalladinite and some unnamed phases enriched with Rh, Ru and Se form inclusions within grains of Pt-Fe alloys (Zaykova et al., 2020).

The grains of Pt-Fe alloys are angular with relics of growth sculpture and imprints of other minerals, probably indicating short distances from their primary source (Zaykova et al., 2020). Inductively-coupled plasma mass spectrometry with laser ablation (LA-ICP-MS) analysis of 5 grains of Pt-Fe alloy from the Kazan placer showed elevated contents of (ppm, mean) As (113), Sb (845), Au (2455), Hg (150), Rh (4640), Pd (460), Os (6890), Ir (6890), Te (1.9), Ag (2.2), Mo (4.2) and elements characteristic of chromite (Cr, Mn, V). Selenium contents were below the limit of detection of about 1 ppm (Artem'ev and Zaykov, 2019).

.

https://doi.org/10.1180/mgm.2022.122 Published online by Cambridge University Press

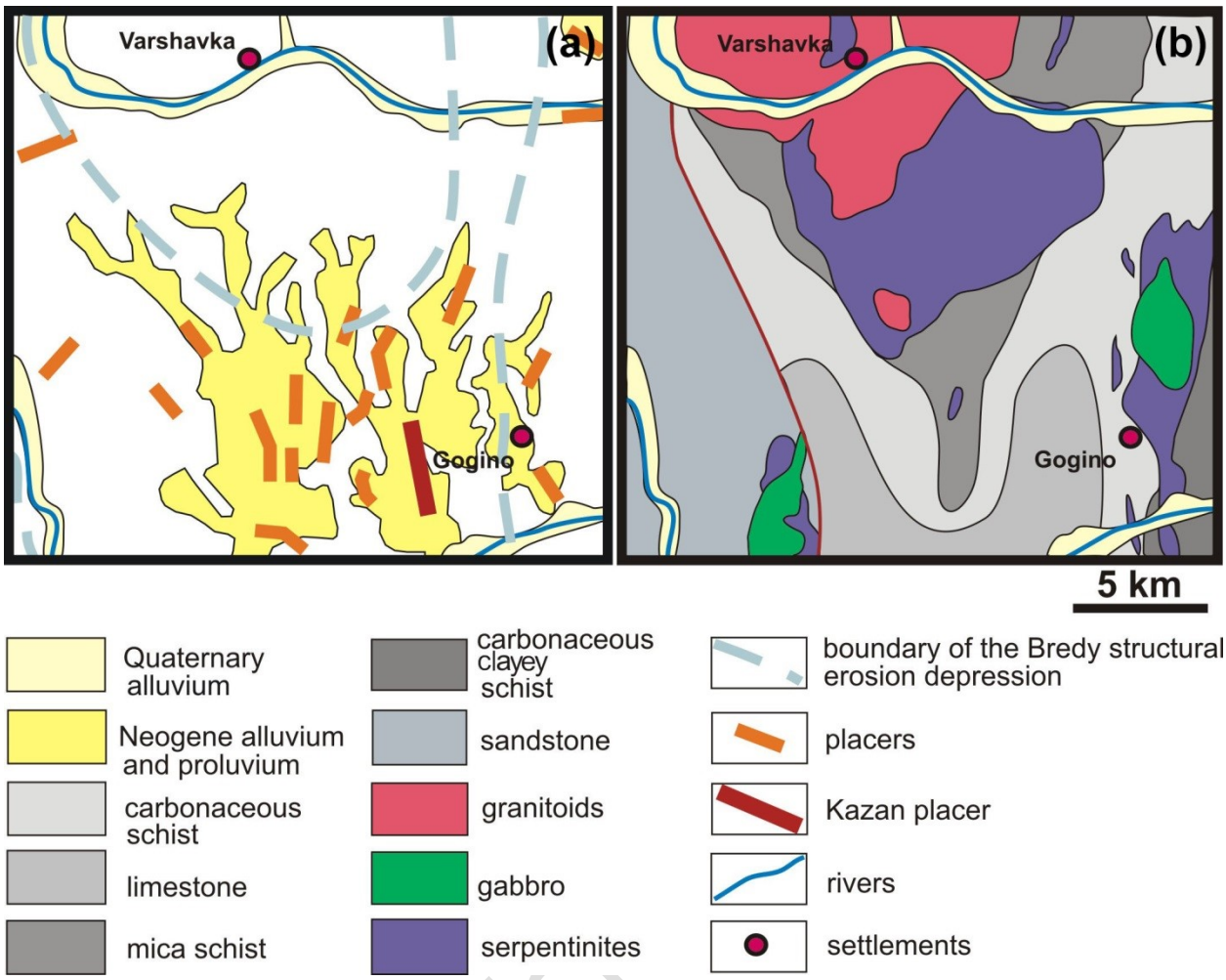

Fig. 2. Position of the Kazan placer on the geological map of the Gogino placer zone within the Bredy structural erosion depression (a) and geological map of the underlying Palaeozoic basement (b).

Results

Morphology, association and physical properties

The studied heavy concentrate consisted of chromite, platinum and gold alloys. Fe-Pt alloy grain with zaykovite inclusions is about 1 mm in size and carries some Cu (Table 1). According to EBSD data the Pt-Fe alloy have a good conformity with isoferroplatinum (ICSD 56275) with mean angle deviation (MAD) of 0.20-0.28° and with platinum (ICSD 76153) with MAD of 0.23-0.4°. The EBSD patterns of isoferroplatinum and platinum are very similar and can not be reliably distinguished purely on EBSD basis, thus we use a Pt-Fe alloys as a name of mineral

https://doi.org/10.1180/mgm.2022.122 Published online by Cambridge University Press

according to (Cabri and Feather, 1975; Cabri et al., 2022). Micron-size inclusions of Au-Pd alloy (Table 2) and Pd-Sb-Te phase (table 3, SC) occur within the studied grain hosting zaykovite. According EBSD the structure of Pd-Sb-Te phase is close to mertieite-II with the MAD of 0.48°.

Table 1. Chemical composition of Pt-Fe alloy grain with zaykovite inclusions (wt.%, EDA)

No	Os	Fe	Pt	Cu	Total	Calculated formulae
1	0.49	6.69	92.19	0.45	99.82	$Pt_{0.78}Fe_{0.20}Cu_{0.01}$
2	-	6.21	93.13	0.71	100.07	$Pt_{0.80}Fe_{0.18}Cu_{0.02}$
3	-	6.75	92.69	0.34	99.81	$Pt_{0.78}Fe_{0.20}Cu_{0.01}$

Notes. Dash – below limit of detection

Table 2. Chemical composition of Au-Pd alloy (wt.%, EDA)

	Pd	Au	Cu	Pt	Ag	total	Calculated formulae
1	8.23	87.04	1.59	2.61	0.43	99.9	$Au_{0.79}Pd_{0.14}Cu_{0.04}Pt_{0.02}Ag_{0.01}$
2	8.34	85.86	1.34	3.76	0.57	99.87	$Au_{0.78}Pd_{0.14}Cu_{0.04}Pt_{0.03}Ag_{0.01}$
3	7.55	84.75	1.47	5.06	0.81	99.64	$Au_{0.77}Pd_{0.13}Cu_{0.05}Pt_{0.03}Ag_{0.01}$
4	9.12	85.90	1.34	2.88	0.43	99.67	$Au_{0.78}Pd_{0.15}Cu_{0.04}Pt_{0.03}Ag_{0.01}$

Table 3. Chemical composition of Pd-Sb-Te phase (wt.%, EDA)

№	Pd	Pt	Ag	Sb	Te	As	Total	Calculated formulae
1	64.09	7.7	-	18.92	9.06	-	99.77	$(Pd_{10.41}Pt_{0.68})_{\Sigma 11.09}(Sb_{2.68}Te_{1.23})_{\Sigma 3.91}$
2	63.72	7.93	-	18.81	9.44	-	99.89	$(Pd_{10.35}Pt_{0.70})_{\Sigma 11.05}(Sb_{2.67}Te_{1.28})_{\Sigma 3.95}$
3	62.88	7.96	1.02	19.35	8.34	-	99.54	$(Pd_{10.24}Pt_{0.71}Ag_{0.16})_{\Sigma 11.11}(Sb_{2.75}Te_{1.13})_{\Sigma 3.88}$
4	61.96	7.98	-	14.11	15.84	-	99.89	$(Pd_{10.12}Pt_{0.71})_{\Sigma 10.83}(Te_{2.16}Sb_{2.01})_{\Sigma 4.17}$
5	61.01	10.35	-	20.25	7.91	-	99.52	$(Pd_{10.06}Pt_{0.93})_{\Sigma 10.99}(Sb_{2.92}Te_{1.09})_{\Sigma 4.01}$
6	61.28	9.7	-	19.63	9.01	-	99.62	$(Pd_{10.07}Pt_{0.87})_{\Sigma 10.94}(Sb_{2.82}Te_{1.24})_{\Sigma 4.06}$
7	61.76	8.22	1.6	18.35	9.56	0.43	99.9	$(Pd_{10.02}Pt_{0.73}Ag_{0.26})_{\Sigma 11.01}(Sb_{2.60}Te_{1.29}As_{0.10})_{\Sigma 3.99}$
8	53.91	19.17	1.11	19.75	5.77	-	99.7	$(Pd_{9.24}Pt_{1.79}Ag_{0.19})_{\Sigma 11.22}(Sb_{2.60}Te_{1.29})_{\Sigma 3.89}$
9	59.79	13.31	-	18.42	7.91	-	99.43	$(Pd_{9.99}Pt_{1.21})_{\Sigma 11.20}(Sb_{2.69}Te_{1.10})_{\Sigma 3.79}$

Notes. Dash – below limit of detection.

Zaykovite was found as elongated idiomorphic crystals up 40 μm in size (Fig. 3). Zaykovite forms intergrowthes with Pd-Sb-Te phase (Fig. 3 d-f) and Au-Pd alloy (Fig. 3 d).

.

https://doi.org/10.1180/mgm.2022.122 Published online by Cambridge University Press

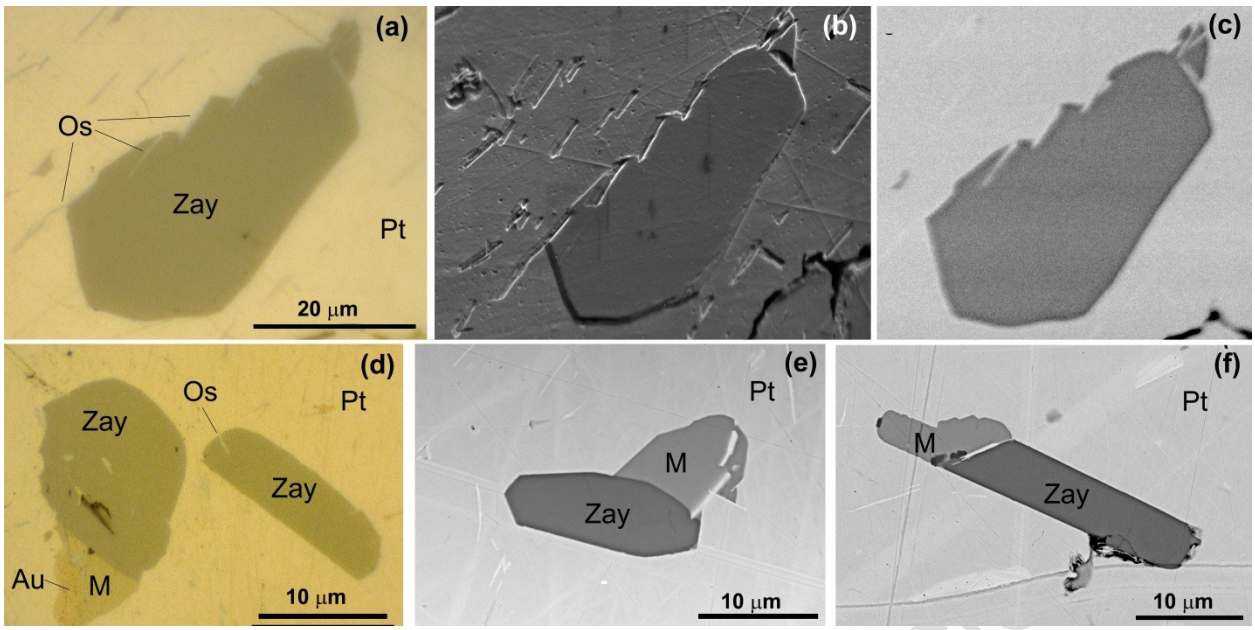

Fig. 3. Morphology of zaykovite (Zay) inclusions in Pt-Fe alloy (Pt). a-c - holotype zaykovite - single crystal with thin osmium lamellae (Os), d – intergrowth with Pd-Sb-Te phase (M) and palladian gold (Au); e, f - intergrowth with Pd-Sb-Te phase (M).

(a, d) Photo in reflected light (oil immersion), (b) SE image tilted to 70 degree of the same area, after argon plasma etching, (c, e, f) BSE images.

Under reflected light, zaykovite is gray with a bluish-greeenish tint in comparison with Pt-Fe alloy. It has a yellow-greenish tint in oil immersion (Figs. 3a, d). Zaykovite has metallic luster and black streak. Polarized light reveals its weak bireflectance and anisotropy, but no internal reflexions. Reflectance values are shown in Table 4. Zaykovite has significantly lower reflectance than kingstonite (Fig. 4).

Zaykovite is slightly harder than Pt-Fe alloy and softer, than native osmium. Mohs hardness is estimated as 5½. Micro-indentation could not be measured because of the small size of all grains excluding holotype which was saved for museum collection. Cleavage was not observed. When preparing a microsample for single crystal diffractometry, brittle tenacity was observed.

Density was calculated on the basis of structural formula and unit cell parameters, and refined from single-crystal data resulting in a value of 8.318 $g \cdot cm^{-3}$. Because of the small grain size the density was not measured directly.

https://doi.org/10.1180/mgm.2022.122 Published online by Cambridge University Press

Zaykovite is non-magnetic.

Table 4. Reflectance values measured in air versus Si reference standard:

R_{max}	R_{min}	λ (nm)	R_{max}	R_{min}	λ(nm)
29.4	28.8	400	32.5	31.3	560
29.5	28.9	420	33.1	31.8	580
29.5	29.1	440	33.4	32.0	589 (COM)
29.9	29.3	460	33.7	32.3	600
30.1	29.3	470 (COM)	34.3	32.9	620
30.2	29.4	480	34.8	33.5	640
30.7	29.7	500	35.1	33.7	650 (COM)
31.3	30.2	520	35.3	34.0	660
31.9	30.7	540	35.8	34.6	680
32.2	31.0	546 (COM)	36.3	35.1	700

.

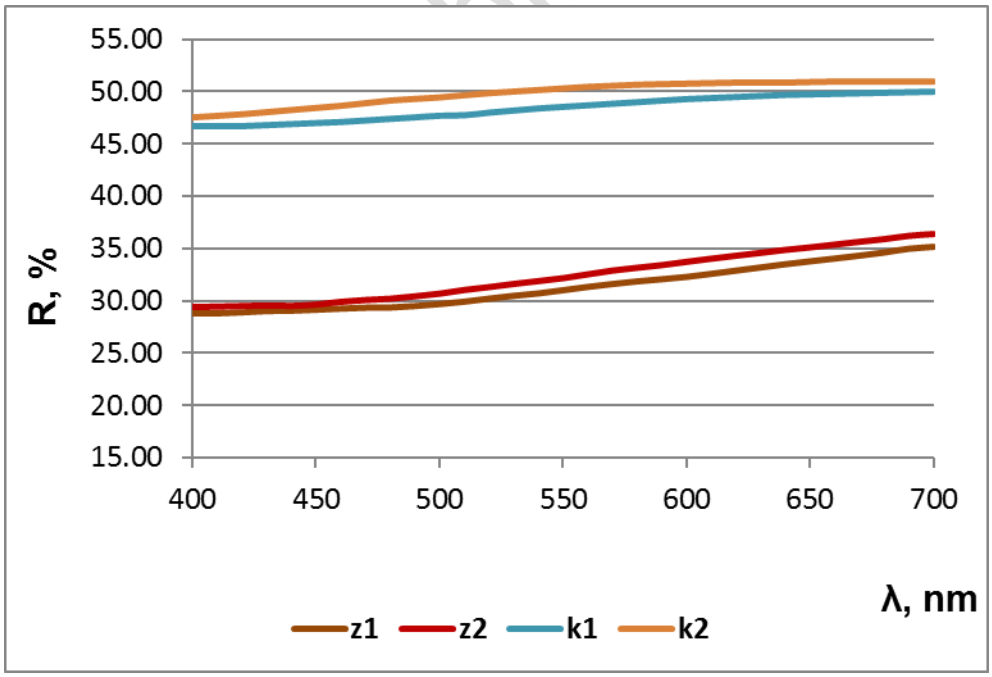

Fig. 4. Reflection spectra of zaykovite (z1, z2) in comparison with kingstonite (k1, k2) (Stanley et al., 2005).

https://doi.org/10.1180/mgm.2022.122 Published online by Cambridge University Press

Chemical composition

Chemical composition of the zaykovite is shown in Table 5. The empirical formula calculated on the basis of 7 atoms per formula unit is $(Rh_{2.26}Pt_{0.46}Ir_{0.25}Ru_{0.01}Pd_{0.01}Fe_{0.01})_{\Sigma 3.00}(Se_{2.77}S_{1.21}Te_{0.02})_{\Sigma 4.00}$.

The simplified formula is $(Rh,Pt,Ir)_3(Se,S)_4$. The ideal formula is Rh_3Se_4, which requires (wt.%): Rh 49.44, Se 50.56.

Distribution of the main elements in the studied grain of Pt-Fe alloy shows that zaykovite is the only compound with Rh and Se (Fig. 5).

Table 5. Chemical composition of the zaykovite holotype (1-5, WDA) and minerals of kingstonite-zaykovite series from the Kazan placer (6-18, EDA) (wt.%).

	Os	Ir	Ru	Rh	Pt	Pd	Fe	S	Se	Te	Total
1	-	7.72	0.20	36.46	14.60	0.18	0.04	6.02	34.92	0.50	100.63
2	-	7.33	0.27	36.74	14.43	0.12	0.05	6.24	35.01	0.46	100.66
3	-	7.70	0.19	36.76	14.92	0.14	0.04	6.24	34.16	0.44	100.58
4	-	7.47	0.22	37.22	14.04	0.08	0.10	6.26	34.90	0.50	100.77
5	-	8.61	0.16	37.32	13.32	0.16	0.05	5.98	34.31	0.33	100.24
mean	-	7.77	0.21	36.90	14.26	0.14	0.06	6.15	34.66	0.45	100.58
6	2.59	5.48	0.40	35.49	8.19	-	0.37	2.17	32.07	13.25	100.00
7	0.21	3.98	0.31	41.53	3.05	0.54	0.14	-	48.85	0.45	96.06
8	-	7.40	-	44.13	1.94	-	-	4.34	42.25	0.83	100.9
9	-	4.16	-	47.28	14.1	-	-	15.25	19.22	-	100.00
10	0.36	0.89	0.47	48.65	12.08	0.61	0.36	12.27	24.29	-	100.00
11	-	12.04	-	36.18	14.23	0.22	0	11.23	25.39	-	99.29
12	-	0.46	0.35	53.44	8.5	-	-	14.57	23.12	-	100.43
13	-	-	0.35	52.26	8.68	-	-	14.65	23.86	0.34	100.13
4	-	7.64	-	52.23	12.52	0.68	0.11	26.64	1.06	-	100.89
15	-	5.19	1.15	55.65	9.58	-	-	24.45	4.1	-	100.11
16	-	7.20	-	58.34	3.94	-	0.24	29.26	1.71	-	100.69
					Calculated formulae (7 apfu)						
1											$(Rh_{2.24}Pt_{0.47}Ir_{0.25}Ru_{0.01}Pd_{0.01}Fe_{0.})_{\Sigma 2.99}(Se_{2.79}S_{1.19}Te_{0.02})_{\Sigma 4.01}$
2											$(Rh_{2.24}Pt_{0.46}Ir_{0.24}Ru_{0.02}Pd_{0.01}Fe_{0.01})_{\Sigma 2.97}(Se_{2.78}S_{1.22}Te_{0.02})_{\Sigma 4.03}$
3											$(Rh_{2.26}Pt_{0.48}Ir_{0.25}Ru_{0.01}Pd_{0.01})_{\Sigma 3.02}(Se_{2.73}S_{1.23}Te_{0.02})_{\Sigma 3.98}$

https://doi.org/10.1180/mgm.2022.122 Published online by Cambridge University Press

4	$(Rh_{2.26}Pt_{0.45}Ir_{0.24}Ru_{0.01}Fe_{0.01})_{\Sigma 2.99}(Se_{2.77}S_{1.22}Te_{0.02})_{\Sigma 4.01}$
5	$(Rh_{2.30}Pt_{0.43}Ir_{0.28}Ru_{0.01}Pd_{0.01}Fe_{0.01})_{\Sigma 3.04}(Se_{2.76}S_{1.18}Te_{0.02})_{\Sigma 3.96}$
mean	$(Rh_{2.26}Pt_{0.46}Ir_{0.25}Ru_{0.01}Pd_{0.01}Fe_{0.01})_{\Sigma 3.00}(Se_{2.77}S_{1.21}Te_{0.02})_{\Sigma 4.00}$
6	$(Rh_{2.37}Pt_{0.29}Ir_{0.38}Ru_{0.03}Fe_{0.05})_{\Sigma 3.02}(Se_{2.79}S_{0.47}Te_{0.71})_{\Sigma 3.98}$
7	$(Rh_{2.63}\ Ir_{0.13}Pt_{0.10}\ Pd_{0.03}Ru_{0.02}Fe_{0.02})_{\Sigma 2.95}(Se_{4.03}Te_{0.02})_{\Sigma 4.05}$
8	$(Rh_{2.60}\ Ir_{0.23}Pt_{0.06})_{\Sigma 2,89}(Se_{3.25}S_{0.82}Te_{0.04})_{\Sigma 4.11}$
9	$(Rh_{2.53}Pt_{0.40}Ir_{0.12})_{\Sigma 3.04}(Se_{2.77}S_{1.21}Te_{0.02})_{\Sigma 3.96}$
10	$(Rh_{2.65}Pt_{0.35}Ir_{0.03}Ru_{0.03}Fe_{0.04}Pd_{0.03})_{\Sigma 3.13}(Se_{2.77}S_{1.21}Te_{0.02})_{\Sigma 3.87}$
11	$(Rh_{2.12}Pt_{0.44}Ir_{0.38}Pd_{0.01})_{\Sigma 2.95}(S_{2.11}Se_{1.94})_{\Sigma 4.05}$
12	$(Rh_{2.76}Pt_{0.23}\ Ru_{0.02}Ir_{0.01})_{\Sigma 3.03}(S_{2.42}Se_{1.56})_{\Sigma 3.97}$
13	$(Rh_{2.70}Pt_{0.24}Ru_{0.01})_{\Sigma 2,95}(S_{2.43}Se_{1.61}Te_{0.01})_{\Sigma 4.05}$
14	$(Rh_{2.43}Pt_{0.31}Ir_{0.19}Pd_{0.03}Fe_{0.01})_{\Sigma 2.96}(S_{2.96}Se_{0.06})_{\Sigma 4.00}$
15	$(Rh_{2.62}Pt_{0.24}Ir_{0.13}Ru_{0.06})_{\Sigma 3.05}(S_{3.70}Se_{0.25})_{\Sigma 3.95}$
16	$(Rh_{2.54}Pt_{0.09}Ir_{0.17}Fe_{0.02})_{\Sigma 2.82}(S_{4.08}Se_{0.10})_{\Sigma 4.18}$

Note. 1-5 – (WDA of holotype), 6-16 EDA. Dash, As, Sb – below limit of detection.

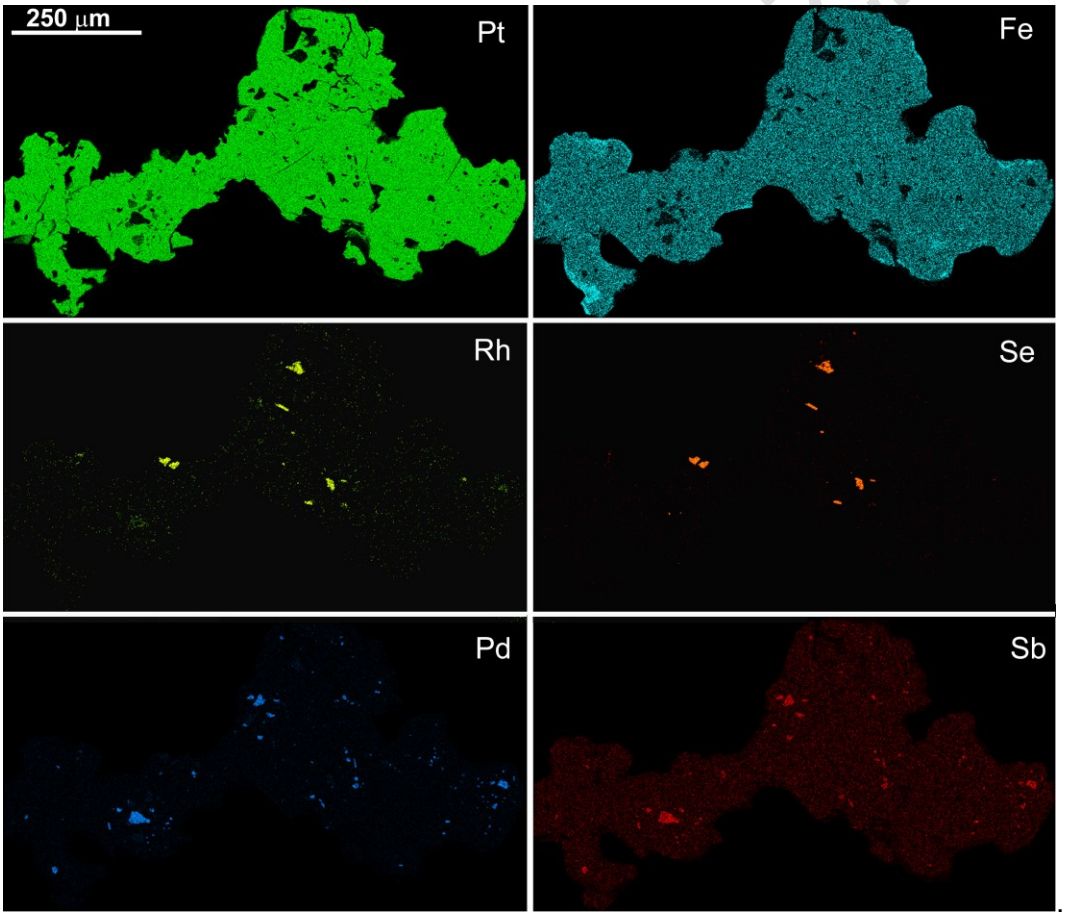

Fig. 5. Elemental distribution EDS maps of Pt-Fe alloy with zaykovite and Pd-Sb-Te phase inclusions.

Crystal structure and X-ray powder diffraction

https://doi.org/10.1180/mgm.2022.122 Published online by Cambridge University Press

Zaykovite crystallizes in the monoclinic system, space group *C*2/*m* (#12). Unit-cell parameters refined from the X-ray single-crystal data: *a* 10.8769(11), *b* 11.1921(11), *c* 6.4796(6) Å, β 108.887(2)°, *V* 746.33(13) Å^3, *Z* = 6. Unit-cell parameters obtained by the refinement of the X-ray powder diffraction data (Table 6): *a* 10.842(13), *b* 11.185(11), *c* 6.463(7) Å; β 108.81(6)°, *V* 741.9(2) Å^3; *Z* = 6. X-ray single-crystal data collection and structure refinement details for zaykovite are summarized in Table 7. Fractional atomic coordinates and displacement parameters in the crystal structure of the mineral are given in Table 8. Selected interatomic bond lengths are presented in Table 9. Zaykovite is a selenium-dominant analogue of kingstonite, Rh_3S_4 (Stanley et al., 2005), and of synthetic kingsonite counterpart (Beck and Hillbert, 2000) (Table 10). In spite that the Rh-Se system was characterized in a wide range of compositions (Rummery and Heyding, 1967), the synthetic analogue of zaykovite, Rh_3Se_4 was not yet known. Therefore, the discovery of zaykovite is a contribution to the crystal chemistry of the Rh-Se system, which now includes 6 structurally confirmed phases (Table 11). As it could be expected, the compounds in this system have many structural analogues in the closely related Rh-S join (Table 11), but the selenide part is more diverse. The pyrite-type RhX_2 phases (*X* = Se or S) are known in both systems (Thomassen, 1929; Rummery and Heyding, 1967; Kjekshus et al., 1979), whereas Rh_3Se_8, with a rhombohedrally distorted pyrite structure (Kjekshus et al., 1979), has no sulfide analogue. The same is true for RhSe, which adopts hexagonal close-packed nickeline structure (Rummery and Heyding, 1967), but its sulfide analogue was not reported.

Zaykovite, as well as kingstonite, have *X*:Rh ratio intermediate between that of bowieite, Rh_2S_3, and miassite, $Rh_{17}S_{15}$ (Table 11). Beck and Hillbert (2000), who provided a detailed description of the crystal structure of synthetic Rh_3S_4 (a kingstonite analogue), showed that it has similarities to the structures of Rh_2S_3 and $Rh_{17}S_{15}$. We highlight the main features of zaykovite structure, which has literally the same topology as of Rh_3S_4 and kingstonite, except for the longer Rh–*X* bond distances due to the domination of Se in the *X*-sites (Table 9). Of four symmetrically independent Rh sites, Rh3 and Rh4 are each coordinated by 6 Se atoms to form distorted octahedra [$RhSe_6$], similar to those in synthetic Rh_2Se_3 (Parthe et al., 1967). The [$RhSe_6$] octahedra are connected via common edges to form 6-membered rings (Figure 6a).

https://doi.org/10.1180/mgm.2022.122 Published online by Cambridge University Press

The coordination of Rh1 and Rh2 sites is more complex – besides Se atoms, each of them is bonded to other Rh atom to form Rh-Rh bonds (Table 9), that results in the creation of the [Rh_6] puckered rings having chair-like conformation (Figure 6b). It is noteworthy that the domains formed by metallic-type Rh–Rh bonds similar to those in zaykovite were reported in $Rh_{17}S_{15}$ – a synthetic analogue of miassite (Schubert, 1977; Britvin et al., 2001). The [Rh_6] puckered rings in the zaykovite structure are arranged into the infinite framework via Se4–Se4 diselenide (pyrite-type) "dumbbell" bridges (Figure 6b). The Se4–Se4 distance in the "zaykovite dumbbell" is 2.409 Å, that is, taking into account partial substitution of Se for S, is almost the same as 2.499 Å in pyrite-type $RhSe_2$ (Kjekshus et al., 1979).

Table 6. X-ray powder diffraction data (*d* in Å) for zaykovite.

I_{meas}	d_{meas}	I_{calc}	d_{calc}	*hkl*	I_{meas}	d_{meas}	I_{calc}	d_{calc}	*hkl*
		5	7.562	110			4	1.928	-403
		3	5.593	020			3	1.886	-351
37	5.43	15	5.428	-111			6	1.872	350
		16	5.131	200	20	1.861	29	1.864	060
		4	4.759	-201			6	1.861	113
		2	4.284	111	22	1.855	43	1.853	-133
		2	4.128	021			8	1.839	-152
		2	3.781	220			6	1.822	-423
		9	3.624	-221			3	1.812	-442
		5	3.425	201			4	1.805	-601
75	3.275	57	3.271	310	12	1.787	15	1.786	-532
100	3.199	100	3.196	-131			4	1.785	242
		8	3.104	-202	16	1.754	17	1.753	-602
87	3.061	64	3.059	002			3	1.752	260
		10	2.921	221			6	1.752	332
		2	2.906	131	8	1.740	4	1.739	-352
28	2.700	14	2.696	-401			7	1.736	-513
		14	2.685	-312	9	1.714	11	1.715	203
19	2.630	6	2.627	112			2	1.713	402
62	2.568	43	2.566	400			6	1.710	600
		29	2.554	-331			7	1.708	351
41	2.545	42	2.543	041			10	1.703	-243
		6	2.521	330	34	1.697	43	1.696	441
31	2.438	13	2.441	-132			3	1.684	133
		14	2.429	-421			2	1.615	-204
34	2.413	18	2.411	-241	7	1.607	7	1.607	531
27	2.321	16	2.319	202			9	1.592	062
		4	2.166	241	13	1.591	4	1.590	-533

https://doi.org/10.1180/mgm.2022.122 Published online by Cambridge University Press

		2	2.157	331	4	1.587	-443
22	2.150	12	2.148	-203	4	1.586	-603
20	2.131	10	2.129	-511	6	1.552	-404
		3	2.105	-151	2	1.547	-171
20	2.100	13	2.098	-113	3	1.533	-461
20	2.076	18	2.078	-242	3	1.532	313
		4	2.064	042	4	1.508	460
		4	2.035	-313	2	1.505	-552
		5	2.019	510	5	1.485	-642
		6	2.015	151	5	1.463	-514
23	2.007	10	2.005	-223	5	1.453	262
		5	2.002	-512	3	1.448	370
		14	1.993	421	3	1.442	153
22	1.955	23	1.954	312	2	1.432	-172
33	1.943	38	1.941	-441	2	1.428	333

https://doi.org/10.1180/mgm.2022.122 Published online by Cambridge University Press

Table 7. Crystal parameters, data collection and structure refinement details for zaykovite

Crystal Data	
Formula *	$(Rh_{2.43}Pt_{0.57})_{\Sigma 3.00}(Se_{2.85}S_{1.16})_{\Sigma 4.00}$
Crystal size (mm)	0.03 × 0.02 × 0.02
Crystal system	Monoclinic
Space group	*C*2/*m*
a (Å)	10.877(1)
b (Å)	11.192(1)
c (Å)	6.4796(6)
β (°)	108.887(2)
V (Å^3)	746.33(12)
Z	6
D_x (g cm^{-3})	8.318
Data collection and refinement	
Radiation	Mo*K*α (λ = 0.71073 Å)
Temperature (*K*)	293
2Θ range (°)	4.00 – 54.00
Total reflections collected	3263
No. unique reflections	858
No. unique observed, $I \geq 2\sigma(I)$	804
h, k, l range	–13→13, –14→14, –8→8
F(000)	1614
μ (mm^{-1})	45.11
No. refined parameters	63
$R_{int.}$	0.024
R_1 [$F \geq 4\sigma(F)$]	0.016
wR_2	0.037
S = *GoF*	1.050
Residuals (e Å^{-3}) (min, max)	–1.29, 0. 93
Data completeness	1.000

Note. * As determined *via* site occupancy refinement.

https://doi.org/10.1180/mgm.2022.122 Published online by Cambridge University Press

Table 8. Fractional atomic coordinates and isotropic displacement parameters (Å^2) for zaykovite

Site [a]	*x*	*y*	*z*	U_{iso}	Occupancy
*M*1 (8*j*)	0.36923(2)	0.14068(3)	0.44995(4)	0.00817(13)	$Rh_{0.71}Pt_{0.29}$
*M*2 (4*i*)	0.35205(4)	0	0.05982(8)	0.0086(2)	$Rh_{0.96}Pt_{0.04}$
*M*3 (2*a*)	0	0	1/2	0.0072(2)	$Rh_{0.87}Pt_{0.13}$
*M*4 (4*h*)	0	0.16106(4)	0	0.00706(18)	$Rh_{0.83}Pt_{0.17}$
*X*1 (4*i*)	0.41600(7)	0	0.73608(13)	0.0089(3)	$Se_{0.64}S_{0.36}$
*X*2 (8*j*)	0.12949(4)	0.15737(4)	0.39186(7)	0.00745(16)	$Se_{0.94}S_{0.06}$
*X*3 (4*i*)	0.11709(7)	0	0.89312(13)	0.0074(3)	$Se_{0.66}S_{0.34}$
*X*4 (8*j*)	0.35468(5)	0.20880(6)	0.09986(9)	0.0085(2)	$Se_{0.55}S_{0.45}$

Note. [a]Site multiplicities and Wyckoff symbols are given in parentheses.

https://doi.org/10.1180/mgm.2022.122 Published online by Cambridge University Press

Table 9. Selected bond lengths (Å) for zaykovite and kingstonite

Bond	Zaykovite	Kingstonite [a]
Rh1–*X*1 [b]	2.3589(7)	2.278(4)
Rh1–*X*2	2.5181(5)	2.366(4)
Rh1–*X*2	2.4799(6)	2.406(4)
Rh1–*X*4	2.3494(7)	2.285(4)
<Rh1–*X*>	2.427	2.334
Rh1–Rh1	2.7054(6)	2.674(2)
Rh1–Rh2	2.9323(6)	2.875(2)
Rh2–*X*1	2.4401(9)	2.365(6)
Rh2–*X*1	2.4144(10)	2.326(6)
Rh2–*X*3	2.4312(9)	2.324(6)
Rh2–*X*4	2.3504(7) ×2	2.278(4) ×2
<Rh2–*X*>	2.397	2.314
Rh3–*X*2	2.4932(5) ×4	2.390(4) ×4
Rh3–*X*3	2.4516(8) ×2	2.355(6) ×2
<Rh3–*X*>	2.479	2.378
Rh4–*X*2	2.4733(5) ×2	2.357(4) ×2
Rh4–*X*3	2.4335(6) ×2	2.337(4) ×2
Rh4–*X*4	2.3876(7) ×2	2.320(4) ×2
<Rh4–*X*>	2.431	2.338
*X*4–*X*4	2.4089(11)	2.237(8)

[a] Stanley et al., 2005. [b] *X* = Se (zaykovite), S (kingstonite).

https://doi.org/10.1180/mgm.2022.122 Published online by Cambridge University Press

Table 10. Comparative crystallographic data for zaykovite, kingstonite and synthetic Rh_3S_4

Mineral	Zaykovite	Kingstonite	Synthetic Rh_3S_4
Ideal formula	Rh_3Se_4	Rh_3S_4	Rh_3S_4
Crystal system	Monoclinic	Monoclinic	Monoclinic
Space group	*C*2/*m*	*C*2/*m*	*C*2/*m*
a, Å	10.8769(11)	10.4616(5)	10.29(2)
b, Å	11.1921(11)	10.7527(5)	10.67(1)
c, Å	6.4796(6)	6.2648(3)	6.212(8)
β, °	108.887(2)	109.000(5)	107.70
V, Å^3	746.33(13)	666.34(1)	649.8(1)
$d_{calc.}$, g/cm^3	8.32	7.52	6.70
Reference	This work	Stanley et al., 2005	Beck & Hillbert, 2000

Table 11. Minerals and structurally confirmed synthetic compounds in the systems Rh–Se and Rh–S.

X:Rh [a]	Rh–Se system		Rh–S system		Structure type	Ref. [b]
	Mineral	Ideal formula		Mineral		
2⅔		Rh_3Se_8			Rh_3Te_8	[1]
2		$RhSe_2$	RhS_2		Pyrite	[1,2]
1½		Rh_2Se_3	Rh_2S_3	Bowieite	Rh_2S_3	[3,4]
1⅓	Zaykovite	Rh_3Se_4	Rh_3S_4	Kingstonite	Rh_3S_4	[5-7]
1		RhSe			NiAs	[8]
0.88		$Rh_{17}Se_{15}$	$Rh_{17}S_{15}$	Miassite	$Pd_{17}Se_{15}$	[5,9-11]

[a] Atomic ratios; *X* = Se or S. [b] References: [1] Kjekshus et al., 1979. [2] Thomassen, 1929. [3] Parthe et al., 1967. [4] Desborough and Criddle, 1984. [5] This work. [6] Beck and Hillbert, 2000. [7] Stanley et al., 2005. [8] Rummery and Heyding, 1967. [9] Schubert, 1977. [10] Geller, 1967. [11] Britvin et al., 2001.

https://doi.org/10.1180/mgm.2022.122 Published online by Cambridge University Press

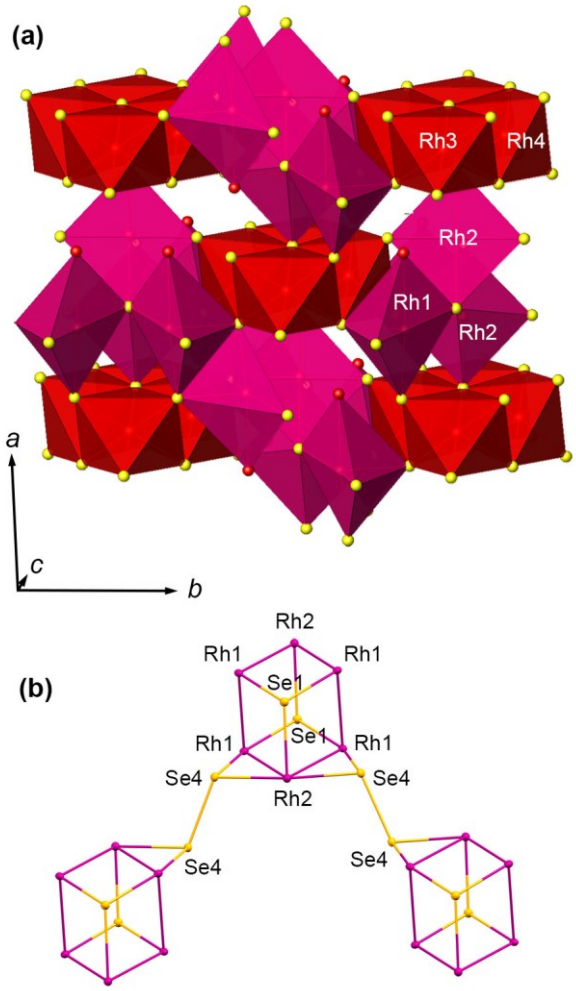

Fig. 6. The crystal structure of zaykovite. (a) Polyhedral representation; a three-dimensional framework composed of two cluster types: (1) Clusters of corner-sharing [Rh($RhSe_4$)] and [$RhSe_5$] distorted square pyramids (coordination around Rh1 and Rh2 atoms) and (2) Clusters of edge-sharing octahedra [$RhSe_6$] (around Rh3 and Rh4 atoms). (b) Ball-and-stick representation of six-membered Rh1-Rh2 clusters, which form pseudo-cubic cages together with Se1 atoms. These clusters are connected in a framework via Se4-Se4 diselenide (pyrite-type) dumbbells. The scale and orientation of structural fragments is the same in (a) and (b).

https://doi.org/10.1180/mgm.2022.122 Published online by Cambridge University Press

The EBSD pattern of zaykovite (Fig. 7a) is well resolved by the theoretical structure of kingstonite (database_code_amcsd 0014575) with the MAD of 0.37° on the basis of maximum of 12 bands (Fig. 7b).

.

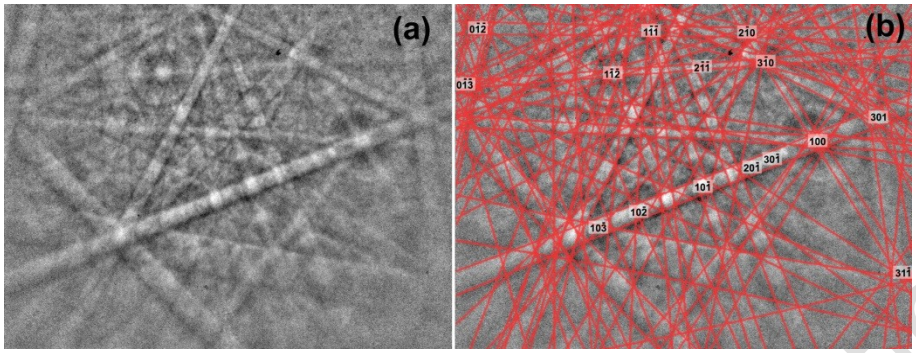

Fig. 7. EBSD pattern of zaykovite (a) and theoretical kingstonite solution fit over the pattern (b).

Contrast of the Kikuchi bands shows that zaykovite forms homogeneous grains with a tendency to form euhedral crystals with pronounced crystallographic facets (fig. 8a). It forms the single crystals, elongated along the [001] axis (Fig. 8b, 9b). The holotype crystal consists of two blocks, which orientation differs by 5.5° (Fig 8c).

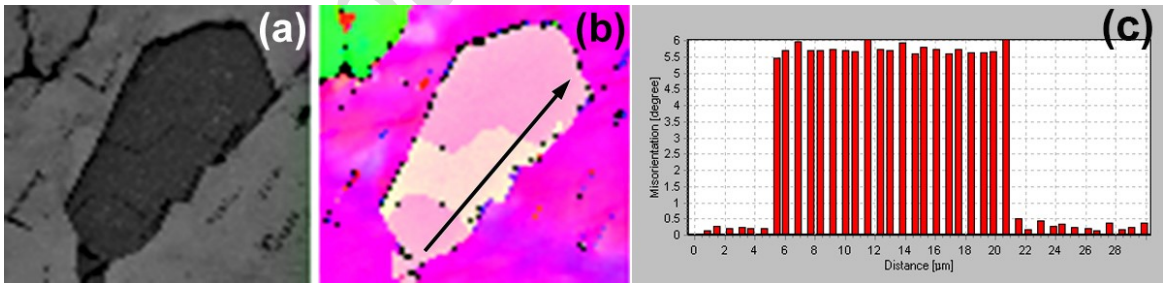

.

Fig. 8. Band contrast (a), orientation in Euler colours (b), and misorientation profile (c) of the holotype zaykovite crystal. Line of profile is shown in (b).

An unexpected result was obtained through EBSD mapping of an area that contains several grains of zaykovite and Pd-Sb-Te phase in an Pt-Fe alloy matrix (fig. 9). While Pd-Sb-Te phase grains have a chaotic orientation typical of late inclusions, three zaykovite grains in two

https://doi.org/10.1180/mgm.2022.122 Published online by Cambridge University Press

different platinum subgrains have the same orientation. The only viable explanation except accidental coincidence is that formation of zaykovite precedes crystallization of Pt-Fe alloy and zaykovite inherits a primary orientation of a protophase. Also, the zaykovite grains manifest ductility, that is seen on the misorientation map as a gradual color change from the point, where the grain contacts with the distorted bands in Pt-Fe alloy. Unfortunately, a potential correlation between zaykovite distortion and distortion of Pd-Sb-Te phase as well as their host Pt-Fe alloy cannot be resolved because of the high degree of the surface distortion during polishing.

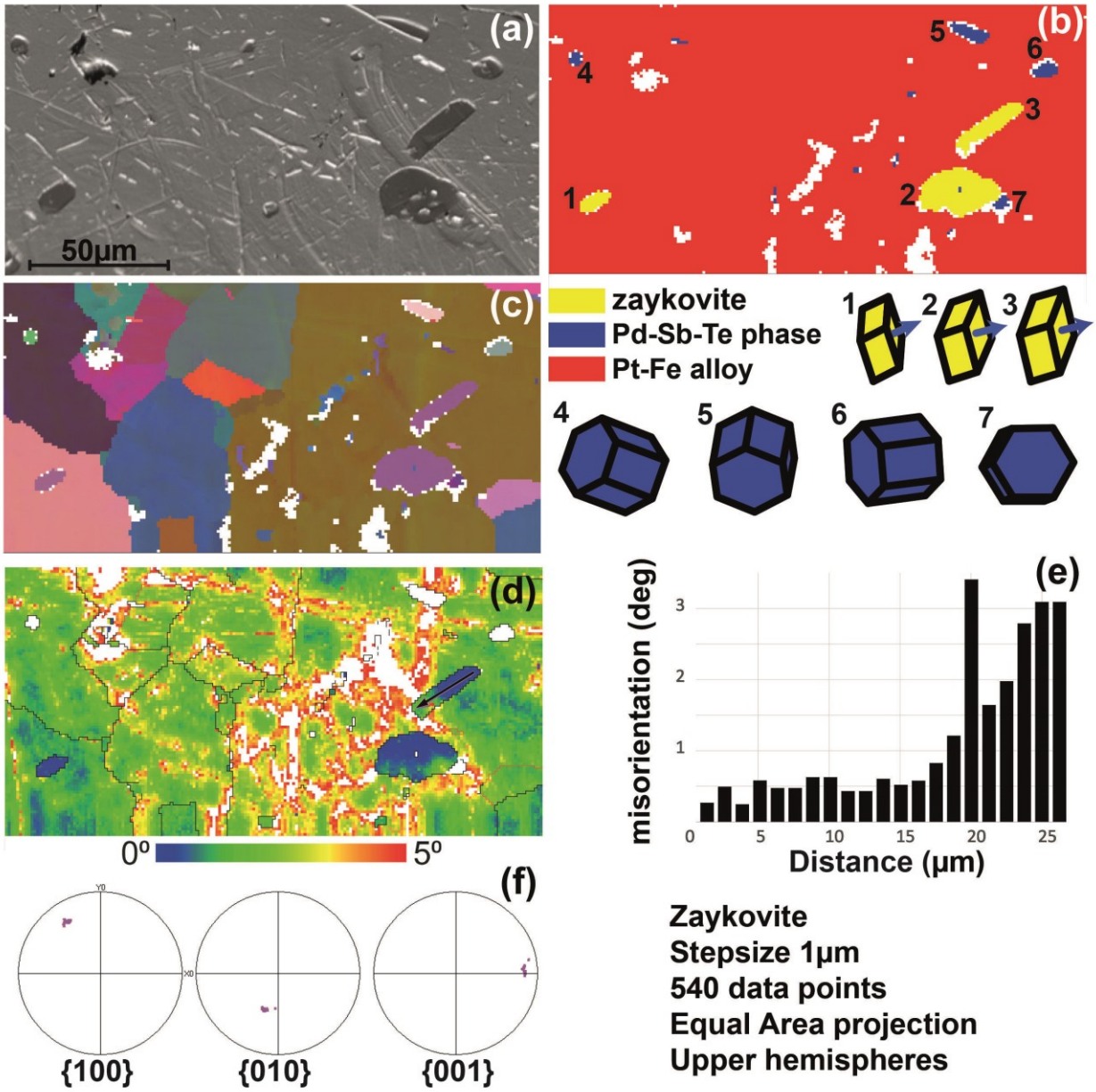

.

https://doi.org/10.1180/mgm.2022.122 Published online by Cambridge University Press

Fig. 9. BSE image (a), phase distribution with orientation of the zaykovite and Pd-Sb-Te grains, blue arrow shows [001] axis of zaykovite (b), and EBSD maps (c-f) of Pt-Fe alloy matrix containing zaykovite and mertieite in Euler angles color scheme with zaykovite cell orientations (c), grains boundaries (d), misorientations profile of the zaykovite grain No.3 (e), and pole figures for zaykovite grains (f).

Discussion

Chemical composition

The chemical composition of selenium-bearing rhodium–dominant sulfides inclusions in Pt-Fe alloy grains of the Kazan placer was analyzed using EDS. (Table 4). The negative correlation between S and Se contents in these inclusions indicates a continuous isomorphic series between kingstonite and zaykovite (Fig. 10).

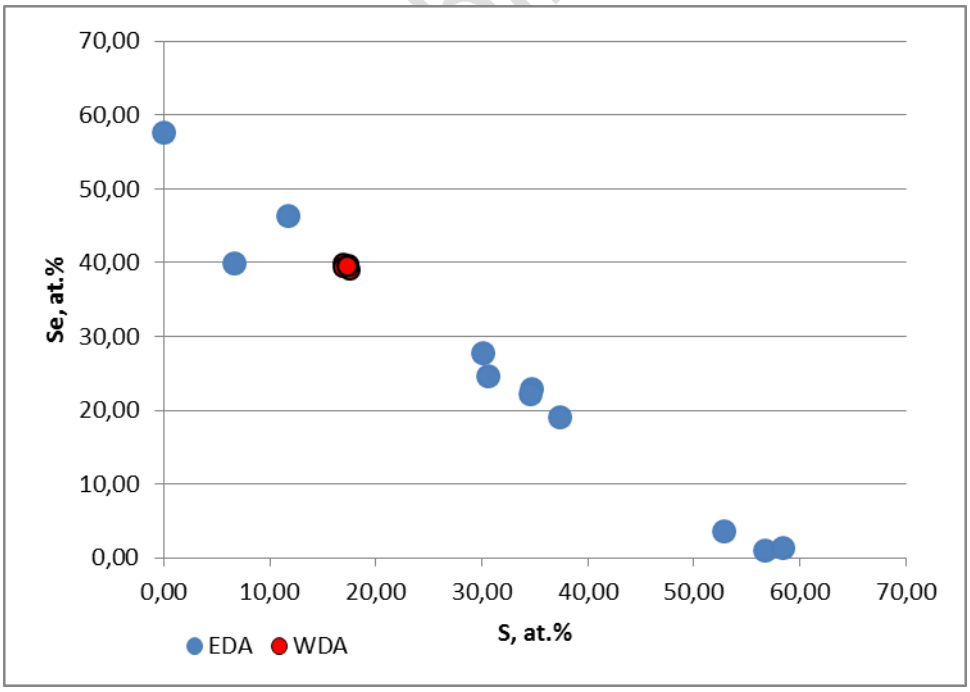

Fig. 10. S-Se plot for the zaykovite-kingstonite series from Kazan placer.

https://doi.org/10.1180/mgm.2022.122 Published online by Cambridge University Press

Origin of the zaykovite

The sources of gold in the placer probably were gold-sulfide and gold-quartz occurences in the Lower Carboniferous sedimentary rocks, represented by carbonaceous and clayey shale, siltstone and limestone (http://www.vsegei.ru). Only the Tambov vein-disseminated gold-sulfide-quartz ore deposit is known in the vicinity of the placer (Podkorytov, 2001).

Sources of PGMs may be the Varshav and Mogutovsky serpentinized dunite-harzburgite massifs, as well as the Gogino gabbro-pyroxenite-dunite zoned massif (Zaykov et al., 2018). However, the finds of laurite, iridium sulfide close to kashinite, and unspecified iridium arsenide were described only for the Vladimir chromite deposit located in the Varshavka massif (Zaykov et al, 2012; Zaykov et al., 2018; Ankushev et al., 2015). It was suggested that the eroded ultramafic massif or its upper part may also be the source of PGM in the Kazan placer.

At present, it is proposed that minerals of the laurite-erlichmanite series, kashinite and some PGE thiospinels are formed at the late stage of magmatic crystallization of PGM in the ultramafic massif (Tolstykh et al., 2011, 2015; Mochalov, 2013). The absence of Se and Rh admixture in Pt-Fe alloy (Artenm'ev, Zaykov, 2019) suggests, that the presence of selenides is not the result of solid solution decomposition.

Based on the euhedral form of the inclusions of bowieite-kashinite and cuprorhodsite in early-formed Pt-Fe alloy grains, their crystallization from melt during the early magmatic stages was suggested (Zaccarini et al., 2018; Stepanov et al., 2020). The thermodynamic advantage of crystallization of Rh_3S_4 in terms of the Gibbs energy minimization in comparison with phases with other Rh:S ratios has been experimentally proven (Jacob & Gupta, 2014). The crystalochemical similarity of selenium and sulfur suggests similar tendency for rhodium selenides.

The crystallization of native osmium, iridium, and laurite from a melt was experimentally confirmed (Brenan and Andrews, 2001). Pronounced euhedral shape of zaykovite indicates its crystallization before or coevally with Pt-Fe alloy. The identical orientations of zaykovite crystals hosted in the different Pt-Fe alloy subgrains also favor the early magmatic crystallization

https://doi.org/10.1180/mgm.2022.122 Published online by Cambridge University Press

hypothesis, assuming that the trapped Os lamellae (Fig. 3) represent the earliest magmatic phase. .

Conclusion

Zaykovite, ideally Rh_3Se_4 was found as inclusion in Pt-Fe alloy grains in heavy mineral concentrate of the Kazan gold placer (South Urals). Zaykovite forms crystals up to 40 μm in size s intergrown with an unnamed Pd-Sb-Te phase and Au-Pd alloy. Its empirical formulae is $(Rh_{2.26}Pt_{0.46}Ir_{0.25}Ru_{0.01}Pd_{0.01}Fe_{0.01})_{\Sigma 3.00}(Se_{2.77}S_{1.21}Te_{0.02})_{\Sigma 4.00.}$ The mineral is gray with black streack and has a metallic lustre. It is the Se analogue of kingstonite with the monoclinic structure and space group C2/m. The crystal structure was solved using single-crystal diffraction data. Unit-cell parameters are a= 10.877(1),b= 11.192(1), c= 6.4796(6) Å,β= 108.887(2). The composition of the studied inclusions in the Pt-Fe alloys grains indicates the existence of a continuous kingstonite-zaykovite serie. The Varshavka and Mogutovsky serpentinized dunite-harzburgite massifs, as well as the Gogino gabbro-pyroxenite-dunite zoned massif could be sources of PGMs including zaykovite in the Kazan placer. The euhedral shape of zaykovite points to its probable crystallization before or simultaneously with Pt-Fe alloy although slightly later than native osmium.

Acknowledgments: The authors are grateful to A.Yu.Ivanov and B.Ya.Hismatullin (“Miass Priisk”) for heavy mineral concentrates from the Kazan placer and Maksim Lozhkin (Nanophotonics Resource Center, SPSU) for preparation of sample surface for EBSD mapping. We also appreciate to Marina Yudovskaya, Oleg Siidra, anonymous reviewer and associate editor Frantisek Laufek for the fruitful comments and linguistic corrections. The work was supported by state contract no. 075-00880-22-00.

Conflicts of Interest: The authors declare no conflict of interest.

Supplementary A. Rh3Se4-cif.pdf

https://doi.org/10.1180/mgm.2022.122 Published online by Cambridge University Press

Supplementary B. Zaykovite_checkcif

Supplementary C. EBSD pattern of mertieite and theoretical mertieite-II solution fit over the pattern.

References

Artem'ev D.A. and Zaykov V.V. (2018) Impurity elements in the native platinum of Kazan placer. Geoarhaeology and archaeological mineralogy-2018: Conference materials. P. 161-164. [In Russian].

Ankushev M. N., Zaykov V. V., Kotlyarov V. A. and Romanenko M. E. (2016) Chrome Spinels and Accessory Mineralization in the Weathering Crust of the Vladimir Deposit, Varshavsky Ultramafic Massif, Southern Urals. *Geology of Ore Deposits,* **58**(8), 697–710.

Bai W., Tao S., Yang J., Fang Q., Shi N. and Li G. (2007) A mineral assemblage of sulfides and sulfo-arsenides from the ophiolite mantle in Tibet. *Acta Petrologica et Mineralogica*, **26**(5), 418–428. [In Chinese].

Barkov A.Y., Nikiforov A.A., Tolstykh N.D., Shvedov G.I. and Korolyuk V.N. (2017) Compounds of Ru-Se-S, alloys of Os-Ir, framboidal Ru nanophases, and laurite-clinochlore intergrowths in the Pados-Tundra complex, Kola Peninsula, Russia. *European Journal of Mineralogy*, **29**(4), 613-621.

Barkov A.Y., Nikiforov A.A., Barkova L.P., Korolyuk V.N. and Martin R.F. (2021) Zones of PGE-Chromite Mineralization in Relation to Crystallization of the Pados-Tundra Ultramafic Complex, Serpentinite Belt, Kola Peninsula, Russia. *Minerals*, **11**(1), 68, doi.org/10.3390/min11010068.

Beck J. and Hillbert T. (2000) Ein ‚altes' Rhodium sulfid mit überraschender Struktur: Synthese, Kristallstruktur und elektronische Eigenschaften von Rh_3S_4. *Zeitschrift für anorganische Chemie*, **626**(1), 72–79.

Belogub E.V., Zaykova E.V., Kotlyarov V.A., Shilovskikh V.V., Britvin S.N. and Pautov L.A. (2019) Selenium in the minerals of the platinum group minerals from gold placer of the

https://doi.org/10.1180/mgm.2022.122 Published online by Cambridge University Press

South Urals. Mineralogical museums: Conference material. Sain-Petersburg, SPbU. 87-89. [In Russian].

Britvin S.N., Rudashevsky N.S., Bogdanova A.N. and Shcherbachev D.K. (1998) Polkanovite $Rh_{12}As_7$ – a new mineral from placers of Miass River, Urals. *Zapiski Vserossiiskogo Mineralogicheskogo Obshchestva*, **127**(2), 60-62. [In Russian].

Britvin S.N., Rudashevsky N.S., Bogdanova A.N. and Shcherbachev D.K. (1999) Palladodymite $(Pd,Rh)_2As$ – a new mineral from placers of Miass River, Urals. *Zapiski Vserossiiskogo Mineralogicheskogo Obshchestva,* **128**(2), 39-42. [In Russian].

Britvin S.N, Rudashevsky N.S., Bogdanova A.N. and Shcherbachev D.K. (2001) Miassite $Rh_{17}S_{15}$ – a new mineral from a placer of Miass River, Urals. *Zapiski Vserossiiskogo Mineralogicheskogo Obshchestva,* **130**(2), 41-45. [In Russian].

Britvin S.N., Dolivo-Dobrovolsky D.V. and Krzhizhanovskaya M.G. (2017) Software for processing the X-ray powder diffraction data obtained from the curved image plate detector of Rigaku RAXIS Rapid II diffractometer. *Zapiski Rossiiskogo Mineralogicheskogo Obshchestva*, **146**(3), 104–107 [In Russian].

Cabri L. and Feather C. (1975) Platinum-iron alloys: a nomenclature based on a study of natural and synthetic alloys. *Canadian Mineralogist*, **13**, 117-126.

Cabri L., Oberthur T. and Schumann D. (2022) The mineralogy of Pt-Fe alloys and phase relations in the Pt-Fe binary system. *Canadian Mineralogist*, **60**, 331-339.

Cook N. J., Wood S. A., Gebert W., Bernhardt H. J. and Medenbach, O. (1994) Crerarite, a new Pt-Bi-Pb-S mineral from the Cu-Ni-PGE deposit at Lac Sheen, Abitibi-Temiscaminque, Quebec, Canada. *Neues Jahrbuch für Mineralogie, Monatshefte,* 567-575.

Davis R.J., Clark A.M. and Criddle A.J. (1977) Palladseite, a new mineral from Itabira, Minas Gerais, Brazil. *Mineralogical Magazine*, **41**, 123.

Desborough G.A. and Criddle A.J. (1984) Bowieite: a new rhodium-iridium-platinum sulfide in platinum-alloy nuggets, Goodnews Bay, Alaska. *Canadian Mineralogist*, **22**, 543-552.

Dolomanov O.V., Bourhis L.J., Gildea R.J., Howard J.A. and Puschmann H. (2009) OLEX2: a complete structure solution, refinement and analysis program, *Journal of Applied Crystallography*, **42**, 339–341.

https://doi.org/10.1180/mgm.2022.122 Published online by Cambridge University Press

Geller S. (1967) The crystal structure of the superconductor $Rh_{17}S_{15}$. *Acta Crystallographica*, **15**, 1198–1201.

ICSD (Inorganic Crystal Structure Database), Fachinformationszentrum (FIZ) Karlsruhe, 2021.

Jacob K.T. and Gupta P. (2014) Gibbs free energy of formation of rhodium sulfides. *The Journal of Chemical Thermodynamics*, **70**, 39-45 .

Jebwab J., Cervelle B., Gouet G., Hubaut X. and Piret P. (1992) The new platinum selenide luberoite Pt_5Se_4 from the Lubero region (Kivu Province, Zaire). *European Journal of Mineralogy*, **4**, 683-692.

Johan Z., Picot P. and Pierrot R. (1970) L'oosterboschite $(Pd,Cu)_7Se_5$, une nouvelle espèce minérale et la trogtalite cupro-palladifère de Musonoï (Katanga). *Bulletin de la Société française de Minéralogie et de Cristallographie,* **93**, 476-481.

Karimova V., Zolotarev A.A., Evstigneeva T.L. and Johanson B.S. (2018) Mertieite-II, $Pd_8Sb_{2.5}As_{0.5}$, crystal-structure refinement and formula revision. *Mineralogical Magazine,* **82**(S1), S247 - S257.

Kjekshus A., Rakke T. and Andresen A.F. (1979) Pyrite like phases in the Rh-Se system. *Acta Chemica Scandinavica*, **A33**, 719–725.

Krivovichev V.G. Mineral species (2021). St.Petersburg Univ. Publ. House. 599 pp. [In Russian].

Malitch K.N., Stepanov S.Yu., Badanina I.Yu. and Khiller V.V. (2015). Assemblages of platinum-group minerals of the Svetlyi Bor, Veresovyi Bor, and Nizhnii Tagil clinopyroxenite–dunite massifs of the Middle Urals. *Vestnik UrO RMO*, **12**, 65–83. [In Russian].

Paar W.H., Roberts A.C., Criddle A.J. and Topa D. (1998) A new mineral, chrisstanleyite, $Ag_2Pd_3Se_4$, from Hope's Nose, Torquay, Devon, England. *Mineralogical Magazine,* **62**(2), 257–264.

Palamarchuk R.S., Stepanov S.Yu., Kozlov A.V., Khanin D.A., Varlamov D.A., Zolotarev A.A., Jr., Kiseleva D.V. and Shilovskikh V.V. (2020) Platinum-group minerals from the Malaya Kamenushka River placer, Middle Urals, Russia. *Mineralogical Magazine*, **84**, 900–912.

Parthe E., Hohnke D. and Hulliger F. (1967) A new structure type with octahedron pairs for Rh_2S_3, Rh_2Se_3 and Ir_2S_3. *Acta Crystallographica*, **23**, 832–840.

https://doi.org/10.1180/mgm.2022.122 Published online by Cambridge University Press

Podkorytov, P.P. Report on geological work at the Tambov gold deposit conducted by Kochkarsky GGP in 1991-1992. and OOO Bredinskaya Gold Mining Company in 1995-2001. [In Russian].

Polekhovskiy Y.S., Tarasova I.P., Nesterov A.P., Pakhomovskiy Y.A. and Bakhchisaraitsev A.Y. (1997) Sudovikovite $PtSe_2$ - a new platinum selenide from Karelia metasomite. *Doklady Akademii Nauk*, **354**, 82-85. [In Russian]

Rakhimov I.R., Saveliev D.E., Salikhov D.N., Vishnevskiy A.V. and Vladimirov A.G. (2021a) Multi-stage magmatic-hydrothermal sulfide-PGE mineralization of the Khudolaz complex (South Urals). *Geology of Ore Deposits*, **63**(4), 341-367.

Rakhimov I.R., Saveliev D.E. and Vishnevskiy A.V. (2021b). Platinum metal mineralization of the South Urals magmatic complexes: geological and geodynamic characteristics of formations, problems of their genesis, and prospects. *Geodynamics and Tectonophysics* **12**(2), 409-434. [In Russian].

Roberts A.C., Paar, W.H., Cooper, M.A., Topa, D., Criddle, A.J. and Jedwab, J. (2002) Verbeekite, monoclinic $PdSe_2$, a new mineral from the Musonoi Cu-Co-Mn-U mine, near Kolwezi, Shaba Province, Democratic Republic of Congo. *Mineralogical Magazine*, **66**, 173-179.

Rummery T. E. and Heyding R. D. (1967) The rhodium/selenium system. *Canadian Journal of Chemistry*, **45,** 131-137.

Saveliev D. E., Zaykov V.V., Kotlyarov V.A., Zaykova E.V. and Kraynev Yu. D. (2017) Chromites and accessory minerals in chromitites and ultramafic rocks of the Nurali massif (the South Urals). Zapiski RMO, 1, 59-84. [In Russian].

Schubert, K. (1977) On the binding in phases of T^{10}-B^6 mixtures. *Acta Crystallographica*, **B33**, 2631–2639.

Sheldrick G.M. (2015) Crystal structure refinement with SHELXL. *Acta Crystallographica*, **C71**, 3–8.

Stanley C. J., Criddle A. J., Spratt J., Roberts A. C., Szymanski J. T. and Welch M. D. (2005) Kingstonite, $(Rh,Ir,Pt)_3S_4$, a new mineral species from Yubdo, Ethiopia, Locality: Bir Bir River, Yubdo District, Wallaga Province, Ethiopia. *Mineralogical Magazine*, **69**, 447-453

https://doi.org/10.1180/mgm.2022.122 Published online by Cambridge University Press

Stepanov S.Yu., Palamarchuk R.S., Kozlov A.V., Khanin D.A., Varlamov D.A. and Kiseleva D.V. (2019) Platinum-Group Minerals of Pt-Placer Deposits Associated with the Svetloborsky Ural-Alaskan Type Massif, Middle Urals, Russia. *Minerals*, **9**, 77, doi:10.3390/min902007.

Stepanov S.Yu., Palamarchuk R.S., Antonov A.V., Kozlov A.V., Varlamov D.A., Khanin D.A. and Zolotarev A.A., Jr. (2020) Morphology Composition, and Ontogenesis of Platinum-Group Minerals in Chromitites of Zoned Clinopyroxenite–Dunite Massifs of the Middle Urals. *Russian Geology and Geophysics*, **61**(1), 47-67.

Thomassen L. (1929) Über Kristallstrukturen einiger binärer Verbindungen der Platinmetalle II. *Zeitschrift für Physikalische Chemie*, **B4**, 277–287.

Tolstykh N.D., Krivenko A.P. and Pospelova L.N. (1997). Unusual compounds of iridium, osmium, and rhutenium with selenium, tellurium, and arsenic from the placers of the Zolotaya River (Western Sayan)]. *Zapiski VMO [Proceedings of the Russian Mineralogical Society],* **6**, 23–34. [In Russian].

Tolstykh N.D., Telegin Yu.M. and Kozlov A.P. (2011) Platinum mineralization of the Svetloborsky and Kamenushinsky massifs (Urals Platinum Belt). *Russian Geology and Geophysics* **52**(6), 603–619.

Tolstykh N., Kozlov A. and Telegin, Yu. (2015). Platinum mineralization of the Svetly Bor and Nizhny Tagil intrusions, Urals Platinum Belt. *Ore Geol. Rev.* **67**, 234–243.

Vymazalová A., Laufek F., Drábek M., Cabral A.R. Haloda J., Sidorinová T., Lehmann B., Galbiatti H.F. and Drahokoupil J. (2012) Jacutingaite, Pt_2HgSe_3, a new platinum-group mineral species from the Cauê iron-ore deposit, Itabira district, Minas Gerais, Brazil. *Canadian Mineralogist*, **50**(2), 431-440.

Zaccarini F., Bindi L., Pushkarev E., Garuti G. and Bakker R.J. (2016) Multi-analytical characterization of minerals of the bowieite-kashinite series from the Svetly Bor complex, Urals, Russia, and comparison with worldwide occurences. *Canadian Mineralogist*, **54**(2), 461–473.

Zaykov V.V., Melekestseva I.Yu., Zaykova E.V., Kotlyarov V.A. and Kraynev, Yu. D. (2017) Gold and platinum group minerals in placers of the South Urals: Composition, microinclusions of ore minerals and primary sources. *Ore geology reviews* **85,** 299**–**320.

https://doi.org/10.1180/mgm.2022.122 Published online by Cambridge University Press

Zaykov V.V., Samoilova O.V., Yuminov A.M. and Belogub E.V. (2011) Laurite and native gold in chromium ores of the Varshavskoe ore field (South Urals). Mineralogy of Urals: materials of the conference, 108-111. [In Russian].

Zaykov V.V., Savel'ev D.E., Kotlyarov V. A., Yuminov A. M., Zherebtcov D. A., Galimov D. M. and Sudarikov M.V. (2012) Platinoids in the cromite ores of the South Urals: data on Karabash, Varshavka and Middle Kraka ultramafic massifs. Metallogeny of the ancient and modern oceans, **18**, 176-182, [In Russian].

Zaykov V.V., Savel'ev D.E. and Zaykova E.V. (2018) The nature of microinclusions of chromspinels in minerals of PGE from the gold placers of South Urals. Notes of the All-Russian Mineralogical Society **147**(5), 27-40. [In Russian].

https://doi.org/10.1180/mgm.2022.122 Published online by Cambridge University Press